

# The IL-1 $\beta$ inhibitor canakinumab in previously treated lower-risk myelodysplastic syndromes: a phase 2 clinical trial

---

Received: 15 July 2024

---

Accepted: 6 November 2024

---

Published online: 13 November 2024

---

 Check for updates

---

A list of authors and their affiliations appears at the end of the paper

In myelodysplastic syndromes (MDS), the IL-1 $\beta$  pathway is upregulated, and previous studies using mouse models of founder MDS mutations demonstrated that it enhances hematopoietic stem and progenitor cells' (HSPCs') aberrant differentiation towards the myeloid lineage at the expense of erythropoiesis. To evaluate whether targeting the IL-1 $\beta$  signaling pathway can rescue ineffective erythropoiesis in patients with MDS, we designed a phase 2 non-randomized single-arm clinical trial (NCT04239157) to assess the safety profile and efficacy of the IL-1 $\beta$  inhibitor canakinumab in previously treated lower-risk MDS patients. We enrolled 25 patients with a median age of 74 years; 60% were male, 16% had lower-risk MDS, 84% had intermediate-1 risk MDS according to the International Prognostic Scoring System score, and 80% failed hypomethylating agent therapy. The study met the primary endpoint of defining the clinical activity of canakinumab, and the secondary objective of determining the safety profile, including the rate of transfusion independence, the duration of response, progression-free survival, leukemia-free survival, and overall survival. The overall response rate was 17.4%, with all responses including hematological improvement. Sequential post-hoc prospective single-cell RNA sequencing analyses of HSPCs and bone marrow mononuclear cells at different time points during therapy showed that canakinumab's on-target effects in hematopoietic populations expressing the IL-1 $\beta$  receptor decreased the TNF-mediated inflammatory signaling pathway but rescued ineffective erythropoiesis only in the context of lower genetic complexity. This study demonstrates that better stratification strategies could target lower-risk MDS patients more effectively.

Increasing evidence supports the role of inflammatory signaling in the pathogenesis of myeloid malignancies, including myelodysplastic syndromes (MDS)<sup>1,2</sup>. Several inflammatory factors, such as IFN- $\gamma$ , IL-1 $\beta$ , and TNF- $\alpha$ , are critical drivers of premalignant clonal expansion, particularly in the setting of clonal hematopoiesis of indeterminate

potential (CHIP) induced by *TET2*- and *DNMT3A*-mutant HSPC clones, which, unlike their healthy counterparts, are intrinsically resistant to inflammation-mediated depletion<sup>3,4</sup>.

Interleukin-1 $\beta$  (IL-1 $\beta$ ) is a proinflammatory cytokine crucial to host-defense responses to infection and injury and activating the

---

✉ e-mail: [scolla@mdanderson.org](mailto:scolla@mdanderson.org)

innate immune system<sup>5</sup>. Secreted IL-1 $\beta$  binds to its receptor (IL-1R1) and triggers a signaling cascade that controls the gene expression of multiple transcription factors, growth factors, and other cytokines involved in hematological functions<sup>6</sup>. Activating this signaling cascade cooperatively induces the expression of canonical IL-1 target genes, such as *IL-6*, *IL-8*, or *IL-1 $\beta$* <sup>7</sup>, which enhances myeloid skewing<sup>8</sup> and results in ineffective erythropoiesis. A deregulated IL-1 $\beta$ -mediated signaling pathway occurs during aging<sup>9</sup> and in many human diseases, including hematopoietic malignancies and cardiovascular disorders<sup>10</sup>. Moreover, recent studies using mouse models of CHIP induced by *Tet2* deletion demonstrated that IL-1 $\beta$  significantly expanded the mutant clone by enhancing *Tet2*-depleted HSPCs' self-renewal capability and inhibiting the demethylation of transcription factor binding sites related to terminal differentiation compared with their wild-type counterparts. More importantly, the genetic deletion of *IL-1r1* in *Tet2*-knockout HSPCs or the pharmacologic inhibition of IL-1 $\beta$  signaling by the IL-1R1 antagonist anakinra reduced myeloid expansion and clonal evolution<sup>11</sup>. These results align with previous results showing that the loss of *IL-1r1* in *Tet2*-knockout HSPCs rescues several abnormalities associated with *Tet2* deficiency, including the expansion of the HSC compartment, the pro-inflammatory state, and the myeloid-lymphoid imbalance<sup>12</sup>. Together, these data underscore the urgent need to clarify whether targeting the IL-1 $\beta$  pathway is a potential intervention strategy to overcome aberrant myeloid differentiation and clonal expansion in human early-stage myeloid neoplasms, such as clonal cytopenias of undetermined significance (CCUS) or lower-risk MDS.

Canakinumab (Novartis, Basel, Switzerland), a fully human monoclonal antibody, targets the IL-1 $\beta$  signaling pathway by blocking the interaction of IL-1 $\beta$  with IL-1R1, thus inhibiting IL-1 $\beta$  downstream target activation and preventing inflammatory mediator production. In the CANTOS (Canakinumab Anti-Inflammatory Thrombosis Outcome Study) trial, canakinumab treatment improved hemoglobin levels and peripheral blood anemia in patients with CHIP-associated mutations, particularly those with *DNMT3A* and *TET2* mutations<sup>13</sup>.

Here, we present the results of a clinical trial evaluating the safety profile and clinical and biological effects of the IL-1 $\beta$  inhibitor canakinumab in patients with lower-risk MDS. Our work demonstrates that canakinumab rescues ineffective erythropoiesis and overcomes transfusion dependency in the context of MDS with lower genetic complexity.

## Results

### Patient cohort

Between August 2020 and June 2023, 27 patients were enrolled in a phase 2 clinical trial of canakinumab. Two patients were ineligible, and 25 received treatment (Fig. 1). After performing a short exploratory dose-finding run-in phase, we found no dose-limiting toxicity, and the recommended phase 2 canakinumab dose was established as 300 mg. The baseline patient characteristics are described in Table 1 and Supplementary Table 1. The cohort's median age was 74 years (range 58–88). Of the 25 patients, 15 (60%) were men, and 22 (88%) were White, one (4%) was Asian, and one (4%) was African American; the race of one patient (4%) was unknown. Five patients (20%) did not receive hypomethylating agent (HMA) therapy, and 20 patients (80%) had failed HMA therapy. Patients who experienced HMA failure received a median number of 6 prior cycles of HMAs (range 4–36); 55% of them had primary HMA therapy failure. Twenty-four patients (96%) had transfusion dependency, defined as the need for transfusion 8 weeks before canakinumab initiation because of a hemoglobin level of less than 8 g/dL. Among patients with transfusion dependency, the median baseline transfusion burden was 3 units of packed red blood cells (PRBCs) per 8 weeks (range 0–16). Fourteen patients (56%) had a normal karyotype, and one patient (4%) had a complex karyotype by conventional cytogenetic analysis. The most common mutations identified by targeted NGS involved *SF3B1* (40%), *TET2* (32%), and

*DNMT3A* (28%). A detailed representation of the clinical characteristics, including the cytogenetic and mutational profiles, of each patient is shown in Supplementary Fig. 1, and detailed information on their molecular profiles is shown in Supplementary Table 2. The BM counts and morphological changes observed during treatment are included in Supplementary Table 3. Five patients (20%) had low (L), six (24%) had moderate low (ML), seven (28%) had moderate high (MH), five (20%) had high (H), and two (8%) had very high (VH) molecular IPSS (IPSS-M) risk.

### Safety profile of canakinumab

Canakinumab demonstrated an overall safe profile in all 25 patients. No patient discontinued therapy, but some non-fatal treatment-emergent adverse events occurred. The most common overall treatment-emergent adverse event was neutropenia. The median duration of grade 3 or higher neutropenia was 14 days (range 5–36), and the median absolute neutrophil count nadir was 0.540 (range 0.150–0.990). One death from sepsis (owing to a lung infection due to methicillin-resistant *Staphylococcus epidermidis*) occurred on day seven after canakinumab initiation and was deemed unrelated to treatment. No patient experienced dose reductions or was removed from the study due to canakinumab-related adverse events. The adverse events that occurred during therapy are summarized in Supplementary Table 4. Patients' hematological parameters at multiple time points during canakinumab treatment are summarized in Supplementary Fig. 2A.

### Efficacy of canakinumab treatment

Of the 25 patients, 23 were evaluable for response (Fig. 2A and Supplementary Table 1). The overall response rate was 17.4% (95% CI 4.9–38.8). Among the 4 responders, 3 failed HMA therapy before study entry. Erythroid and platelet hematological improvement (HI-E and HI-P) were observed in three patients (13%) and one patient (4%), respectively. The HI rate (including HI-E and HI-P) was 17.4% (95% credible interval [7.1% and 37.4%, respectively], based on a Bayesian prior distribution of Beta [1.0, 1.0]). Hematological improvement was exploratorily reassessed according to the IWG 2018 guidelines, and the HI-E was 13.8% (95% credible interval [4.0%, 28.2%]) (Supplementary Table 5). The four patients' response durations were 12.9, 12.1, 5.1, and 3.1 months, respectively. Transfusion independence (TI) was achieved in three patients whose median duration of response was 8.53 months (95% CI 0.41–16.1). Two patients (UPN-01 and UPN-02), including one patient who was highly transfusion-dependent and who received more than six units of PRBC before canakinumab therapy initiation, had a stable response for over 12 months (Supplementary Table 5). Thirteen patients (56.5%) had stable disease, but in six patients (26.1%), the disease progressed during therapy, and of these six patients, one patient developed acute myeloid leukemia at disease progression (Fig. 2A).

After a median follow-up of 24.9 months (95% CI 19.4, not estimable [NE]), the median OS for the entire cohort was 17.3 months (95% CI 14.3, NE), the median PFS was 17.3 months (95% CI 7.73, NE) (Supplementary Fig. 2B, C), and the median LFS was 16.3 months (95% CI: 14.3, NE). When patients were stratified by HMA therapy status, the median OS was 29.4 months (95% CI 16.34, NE) in the HMA-naïve cohort ( $n = 5$ ) and 17.3 months (95% CI 9.67, NE) in the HMA failure cohort ( $n = 20$ ;  $P = 0.64$ ) (Fig. 2B).

Patients were further classified according to the IPSS-M into higher-risk (HR [VH, MH, and H]) and lower-risk (LR [ML and L]) cohorts. All patients with progressive disease (PD) were HR by IPSS-M (42.8% vs. 0%,  $P = 0.01$ ), while all responders (HI) were LR by IPSS-M (36.3% vs. 0%,  $P = 0.01$ ). When we performed a separate univariate analysis to evaluate any associations between the IPSS-M classification and OS or PFS (Fig. 2C), the median OS for the HR IPSS-M and LR IPSS-M groups were 14.3 months and 29.4 months, respectively ( $P = 0.03$ ).

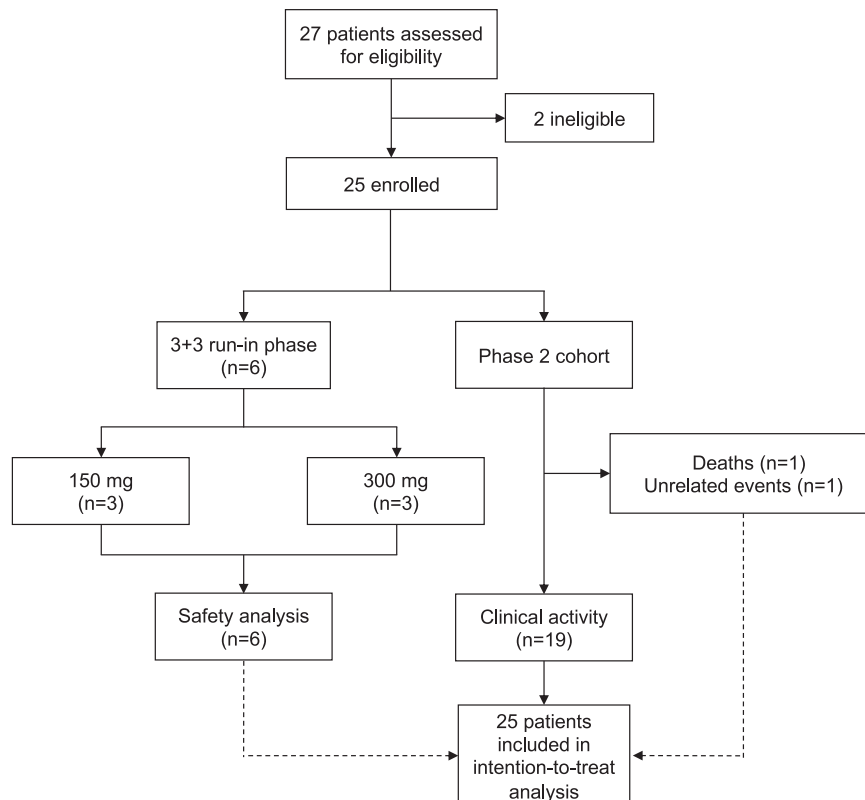


**Fig. 1 | Schematic of the clinical trial.** The diagram summarizes the flowchart of the clinical trial.

Moreover, the HR IPSS-M and LR IPSS-M groups had 1-year PFS rates of 42.9% and 80.0%, respectively ( $P = 0.0087$ ) (Fig. 2C). The significant association between IPSS-M risk category and OS ( $P = 0.04$ ) and PFS ( $P = 0.01$ ) was further confirmed using the Cox proportional hazards model, accounting for age and prior HMA treatment status (Supplementary Table 6).

### Canakinumab induces HSPCs' differentiation in patients with MDS

To evaluate the biological effects of canakinumab on hematopoiesis, we performed sequential post-hoc scRNA-seq analysis of Lin<sup>+</sup>CD34<sup>+</sup> HSPCs obtained before and during treatment from a representative patient with a *DNMT3A* mutation (UPN-02), who had stable Ht-E after two cycles of canakinumab (Fig. 3A, B and Supplementary Data 1). This analysis revealed that canakinumab increased HSCs' differentiation towards the erythroid and myeloid lineage (Fig. 3C). Differential expression analysis revealed that genes involved in the NF- $\kappa$ B signaling pathway, including *IL-1 $\beta$* , *CXCL2*, *CXCL3*, and *MIF*, were significantly downregulated in HSCs obtained at canakinumab response compared with those in HSCs obtained before treatment (Fig. 3D, Supplementary Fig 3A, B, and Supplementary Data 2). Given that HSCs expressed *IL-1 $\beta$*  and *IL-1R1* (Supplementary Fig 3C), these data confirmed canakinumab's on-target engagement. ScRNA-seq analysis of MNCs obtained before and after canakinumab administration (Fig. 3E; Supplementary Data 3) revealed that the expression of major regulators of the NF- $\kappa$ B and inflammatory signaling pathways in MDS, including *TLR2*, *KDM6B*, *REL*, and *NLRP3*, were significantly downregulated in the monocyte population (Fig. 3F, Supplementary Data 4 and Supplementary Fig 3D), which also expressed *IL-1 $\beta$*  and *IL-1R1* (Supplementary Fig 3E). Consistent with this observation, the levels of several pro-inflammatory cytokines, including IL-1 $\beta$ , IL-18, IL-6, and IFN- $\gamma$ , were reduced in BM plasma collected at the time of canakinumab response compared with those in BM plasma collected before treatment (Supplementary Fig 4). This broad spectrum

of pro-inflammatory cytokine inhibition was associated with a recovery of BM erythroblasts (12% vs. 32%; Supplementary Table 3) and significant changes in the immune microenvironment, including a decrease in the CD8<sup>+</sup>GZMK<sup>+</sup> memory T-cell population (Fig. 3G and Supplementary Fig 5A–C), which is associated with several inflammatory conditions and further enhances the release of pro-inflammatory cytokines<sup>14–16</sup>. Consistent with this observation, when we inferred cell-to-cell communication from the combined expression of multi-subunit ligand–receptor complexes using CellPhoneDB<sup>17</sup>, we observed that before canakinumab treatment, CD8<sup>+</sup>GZMK<sup>+</sup> T cells were predicted to interact with the monocyte population significantly, and these interactions were significantly inhibited by canakinumab (Supplementary Fig 5D). Specifically, the expression levels of ligands and receptors known to drive monocyte migration (e.g., *a4b1:PLAUR*, *CCL3/CCL3L1/CCL5:CCR1*)<sup>18–20</sup> and differentiation into highly pro-inflammatory macrophages (e.g., IFN- $\gamma$ :IFNR, *LTB:LTBR*)<sup>21,22</sup> were significantly decreased after treatment (Supplementary Fig 5E, Supplementary Data 5).

Further analyses showed that canakinumab treatment did not rescue aberrant erythroid differentiation in lower-risk MDS patients with *SF3B1* mutations (40% of the patients in our cohort), as demonstrated by scRNA-seq analyses of Lin<sup>+</sup>CD34<sup>+</sup> HSPCs (Fig. 4A, B; Supplementary Data 6) and MNCs (Fig. 4C, D; Supplementary Data 7) isolated from 2 representative patients with *SF3B1* mutations whose best response was stable disease (UPN-07 and UPN-14). Given that *IL-1 $\beta$*  was expressed in both HSCs and monocytes (Supplementary Fig 6A) and that canakinumab significantly decreased NF- $\kappa$ B-mediated inflammatory signaling in these populations (Fig. 4E, F; Supplementary Data 8, 9), these data suggest that the IL-1 $\beta$ -mediated inflammatory pathway does not drive the ineffective erythropoiesis induced by *SF3B1* mutations. Similar data were obtained for 2 other patients with splicing factor mutations whose disease progressed after canakinumab therapy (UPN-12 and UPN-20) (Supplementary Fig 6B–E; Supplementary Data 10–12).

**Table 1 | Characteristics of the 25 patients enrolled in the canakinumab trial**

Characteristic	
Age, y, median (range)	74 (58–88)
Male, n (%)	15 (60)
Hemoglobin, g/dL, median (range)	8.2 (6.6–9.5)
WBC × 10 <sup>9</sup> /L, median (range)	3.2 (2.2–5.9)
ANC × 10 <sup>9</sup> /L, median (range)	1.7 (0.38–3.96)
Platelets × 10 <sup>9</sup> /L, median (range)	129 (16–430.0)
Bone marrow blast %, median (range)	2 (1–4)
WHO 2022 diagnosis, n (%)	
MDS-LB	12 (48)
MDS-SF3B1	11 (44)
MDS-5q	1 (4)
MDS-f	1 (4)
IPSS, n (%)	
Low	4 (16)
Intermediate-1	21 (84)
IPSS-R, n (%)	
Low	12 (48)
Intermediate	12 (48)
High	1 (4)
IPSS-M, n (%)	
Low	5 (20)
Moderate low	6 (24)
Moderate high	7 (28)
High	5 (20)
Very high	2 (8)
Number of mutations per patient, median (range)	3 (1–10)
Number of pre-treatment PRBC units <sup>a</sup> , median (range)	3 (0–16)
Transfusion dependency, n (%)	24 (96)
Prior HMA treatment, n (%)	20 (80)
Number of prior lines of therapy, median (range)	2 (1–5)

Data are median (range), n (%), or n/N (%). WBC white blood cells, ANC absolute neutrophil counts, WHO World Health Organization, MDS-LB MDS with low blasts, MDS-5q MDS with low blasts and isolated 5q deletion, MDS-SF3B1 MDS with low blasts and SF3B1 mutation, MDS-f MDS with fibrosis, Complex ≥ 3 alterations, Mutations ≥ 5% percentage, HMA hypomethylating agent, PRBC packed red blood cell, IPSS International Prognostic Scoring System, IPSS-R Revised International Prognostic Scoring System, IPSS-M Molecular International Prognostic Scoring System.  
<sup>a</sup>Baseline transfusion status was defined during the 8-week period prior to canakinumab initiation.

Discussion

Extensive preclinical studies using mouse models of early-stage MDS demonstrated that genetically and pharmacologically targeting the IL-1β inflammatory signaling pathway rescues aberrant myeloid differentiation, overcomes ineffective erythropoiesis, and arrests clonal expansion<sup>11,12</sup>. To validate these results in the human setting, we conducted a clinical trial of the IL-1β inhibitor canakinumab in patients with lower-risk MDS.

Canakinumab was safe and well-tolerated, with no dose reductions or treatment discontinuation during the study. Cytopenia (occurring in 64% of patients) was the most common grade 3 or higher treatment-emergent adverse event, which may reflect a combination of heightened myelosuppression induced by the treatment or simply the natural history of patients with lower-risk MDS. In contrast to

previous clinical trials in the setting of chronic inflammatory diseases, no grade 3 or 4 infection events were observed<sup>23,24</sup>.

It is worth noting that we initially used the IPSS and IPSS-R criteria<sup>25,26</sup> and defined our patients’ risk as lower-risk MDS because of these patients’ baseline single cytopenias, low number of blasts, lower frequencies of *TP53* mutations (*n* = 2,8%), and complex karyotype (*n* = 1,4%). However, 80% of patients previously received other therapies, including HMA therapy (median number of cycles = 6). The overall median number of prior lines of therapies was 2 (interquartile range 1–3). In addition, 80% of the patients were transfusion-dependent. When patients were re-classified according to the IPSS-M score system<sup>27</sup>, we found that 56% of patients had features of higher-risk disease and were in the MH, H, and VH subgroups. Notably, the IPSS-M score stratification in lower-risk and higher-risk diseases remained significantly associated with OS and PFS.

Canakinumab elicited an overall response rate of 17% (13% HI-E and 4% HI-P), with a median response duration of 8.5 months among responders. We acknowledge the advantages of the IWG 2018 criteria, particularly in refining transfusion burden assessment and hematologic improvement in lower-risk MDS. Although our trial was designed before 2018 using IWG 2006 response criteria, we retrospectively collected transfusion burden data for 16 weeks before canakinumab initiation when possible. The re-analysis with IWG 2018 criteria confirmed that three of four patients who achieved HI maintained responses beyond 16 weeks. However, due to the shortcomings of retrospective data collection, we adhered to the response criteria outlined in our original protocol.

All patients whose disease responded to canakinumab belonged to the lower-risk group by IPSS-M (HI: 36.4%; 4/11), whereas all patients whose disease progressed during treatment were in the higher-risk group (43%, 6/14). Interestingly, the only two patients with HI-E for over 12 months and red blood cell TI (UPN-01 and UPN-02) harbored founder *TET2* or *DNMT3A* mutations, respectively.

Patients with *SF3B1* mutations (40% of the patients in our cohort) did not respond to canakinumab. These results are consistent with the different pathogenic mechanisms of ineffective erythropoiesis caused by *SF3B1* mutations, which induce the aberrant splicing of heme transporters in the mitochondria of erythroblastic cells<sup>28</sup>. Lower HLA-DR expression levels in *SF3B1* mutant monocytes<sup>29</sup> may also affect canakinumab’s efficacy in reducing the interactions with CD8<sup>+</sup>GZMK<sup>+</sup> T cells, which is predicted to drive monocytes’ migration and differentiation into highly pro-inflammatory macrophages. In addition, previous studies showed that *SF3B1*-mutant MDS have lower inflammatory signatures (including lower levels of IL-1β) compared to lower-risk MDS without *SF3B1* mutations, particularly those with isolated 5q deletion, which are predicted to respond to anti-inflammatory therapy<sup>30</sup>. Consistent with these findings, canakinumab treatment was associated with prolonged response and transfusion independence in the one patient with MDS-5q (UPN-01) included in our study.

Resistance to canakinumab treatment was also associated with high genetic complexity, which suggests that beyond inflammation, other intrinsic factors (e.g., cooperative mutation effects) and extrinsic factors (e.g., the exacerbation of immune suppression) contribute to patients’ cytopenias and mutant cells’ clonal expansion.

Consistent with preclinical studies in mice<sup>11</sup>, our study shows that pharmacologically targeting the IL-1β pathway represents a promising therapeutic strategy for improving hematologic parameters and reducing inflammatory cytokine levels in patients with early-stage disease (Supplementary Fig 7).

Given the accumulating evidence of innate immune activation in the pathobiology of MDS and its inflammatory BM microenvironment, particularly in the early stage of the disease, combinations of canakinumab with other anti-inflammasome inhibitors, such as those targeting the NLRP1- or NLRP3-mediated pathways, which neutralize the

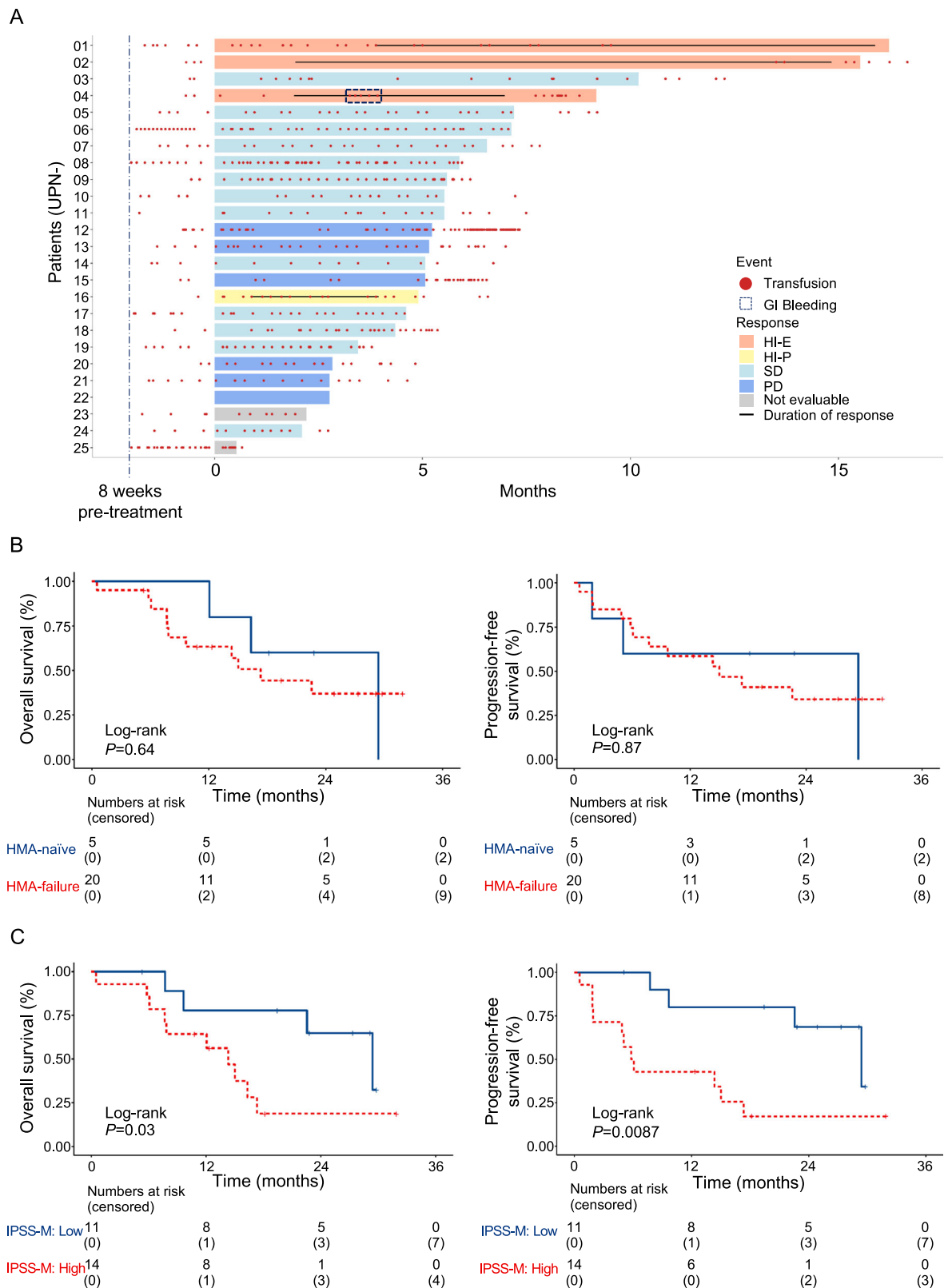
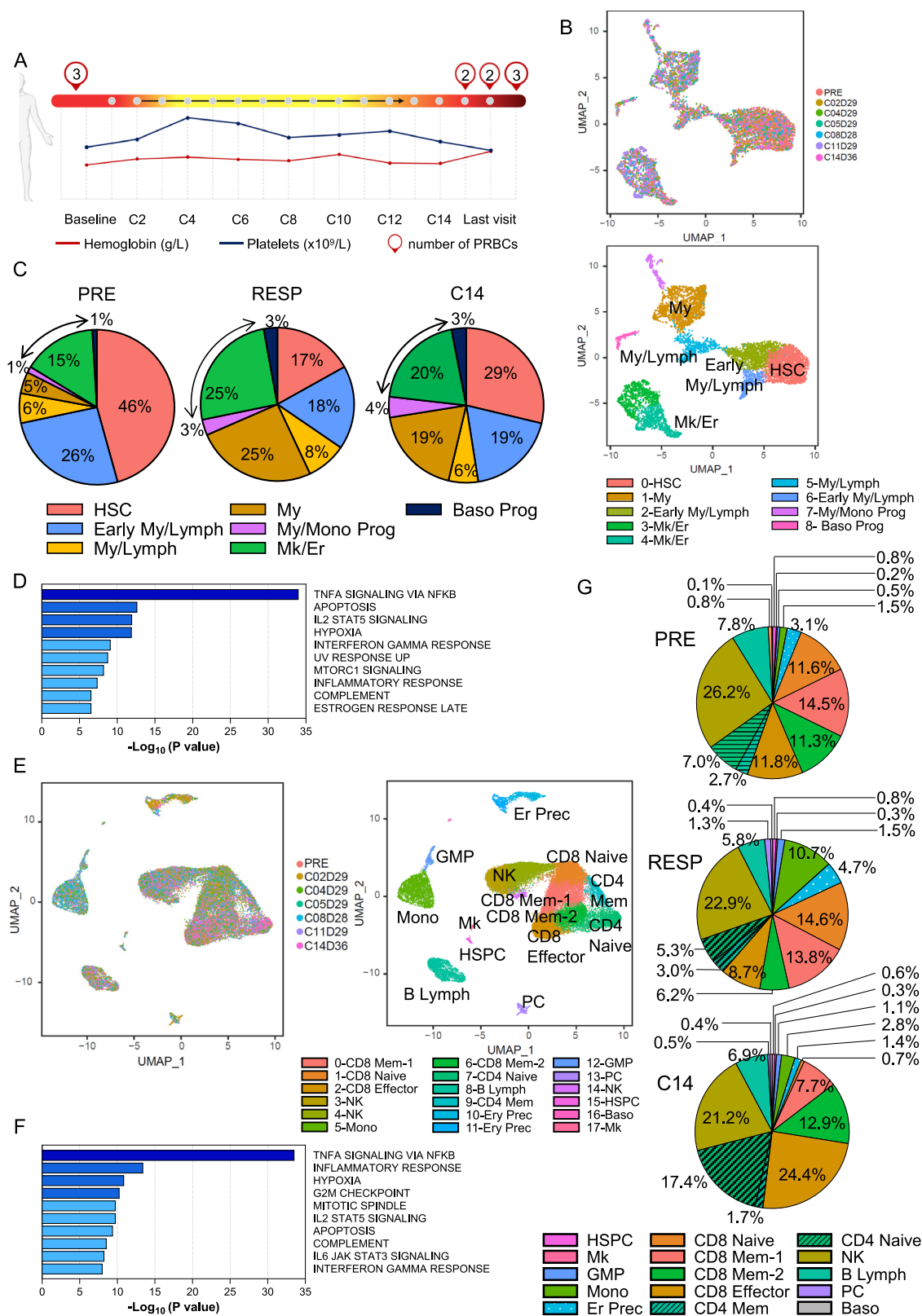


**Fig. 2 | Efficacy of canakinumab in lower-risk MDS patients.** **A** Swimmer's plot showing transfusions, treatment durations, and responses of MDS patients enrolled in the canakinumab trial ( $n=25$ ). Red dots represent independent evaluations of transfusion needs in each patient; the dotted square represents the GI bleeding time in patient UPN-04. GI, gastrointestinal; black lines represent the duration of response. HI-E, hematological improvement-erythroid; HI-P, hematological

improvement-platelets; SD, stable disease; PD, progressive disease.

**B** Kaplan-Meier survival estimate curves for overall survival (left) and progression-free survival (right) stratified by HMA therapy status. **C** Kaplan-Meier survival estimate curves for overall survival (left) and progression-free survival (right) stratified by IPSS-M risk. Source data are provided as a Source Data file.





pyroptotic cell death<sup>31</sup> and erythropoietin elaboration<sup>32</sup> induced by high levels of the alarmin S100A9 observed in the BM of lower-risk MDS patients, may be beneficial in overcoming ineffective erythropoiesis in these patients.

This work has limitations inherent to an early dose-finding study, including the need for a control group and a small sample size. Acknowledging that our patient cohort may not recapitulate the

broader lower-risk MDS population is also essential. The enrollment of patients who were previously heavily treated and/or with high-risk genetic features may not be optimal for evaluating response to IL-1 $\beta$  inhibition. Indeed, although canakinumab demonstrated an efficient on-target effect at the administered dose, our findings suggest its efficacy is limited to patients with lower genetic complexity. Therefore, future studies should consider the stratification of the patients based

**Fig. 3 | Targeting the IL-1 $\beta$  pathway overcomes ineffective erythropoiesis in lower-risk-MDS. A** Schematic of hemoglobin and platelet levels in patient UPN-02 and the number of packed red blood cell (PRBC) units received before and after therapy. The black arrow indicates the response duration. C, cycle. Created in BioRender. Rodríguez-Sevilla, J.J., (2024) <https://www.biorender.com/t63n194>. **B** UMAP plot of scRNA-seq data from Lin<sup>+</sup>CD34<sup>+</sup> cells from the BM of patient UPN-02 before (PRE;  $n = 1381$ ) and after 2, 4, 5, 8, 11, and 14 cycles of canakinumab treatment ( $n = 5721$ ). Different colors represent the sample (left) and cluster (right) identities. My, myeloid; Lymph, lymphoid; HSC, hematopoietic stem cell; Mk, megakaryocytic; Er, erythroid. **C** Cluster distribution of Lin<sup>+</sup>CD34<sup>+</sup> cells from the BM before canakinumab treatment (PRE) and at the time of response (cycles 2, 4, 5, 8, and 11) or relapse (cycle 14), represented as the percentage of cells in each cluster. Black arrows indicate the Mk/Er clusters. RESP, response. For the Mk/Er clusters, comparing samples C2, C4, C5, C8, C11, and C14 to the PRE sample:  $P = 0.92$ ,  $0.00077$ ,  $4.57 \times 10^{-6}$ ,  $0.097$ ,  $1.06 \times 10^{-45}$ , and  $0.0015$ , respectively; two-sided Chi-square test. **D** Pathway enrichment analysis of genes significantly ( $P \leq 0.05$ ) downregulated in HSCs after 2 cycles of canakinumab treatment compared with

those before treatment. The top 10 Hallmark gene sets are shown. **E** UMAP plot of scRNA-seq data from BM MNCs isolated from patient UPN-02 before canakinumab treatment (PRE;  $n = 2980$ ) and after 2, 4, 5, 8, 11, and 14 cycles of treatment ( $n = 27,913$ ). Different colors represent the sample (left) and cluster (right) identities. **F** Pathway enrichment analysis of genes significantly ( $P \leq 0.05$ ) downregulated in monocytes after 2 cycles of canakinumab treatment compared with those before treatment. The top 10 Hallmark gene sets are shown. **G** Cluster distribution of BM MNCs before canakinumab treatment (PRE), at the time of response (cycles 2, 4, 5, 8, and 11) or relapse (cycle 14), represented as the percentage of cells in each cluster. For the memory-2 T cell cluster, comparing samples C2, C4, C5, C8, C11, and C14 to the PRE sample:  $P = 7.49 \times 10^{-27}$ ,  $1.50 \times 10^{-7}$ ,  $0.021$ ,  $1.22 \times 10^{-30}$ ,  $7.67 \times 10^{-30}$ , and  $0.036$ , respectively; two-sided Chi-square test. HSPC, hematopoietic stem and progenitor cell; Mk, megakaryocytic; GMP, granulomonocytic progenitor; Mono, monocytic; Er, erythroid; Prec, precursor; NK, natural killer; Lymph, lymphoid; PC, plasma cell; Baso, basophil; mem, memory; RESP, response. Source data are provided as a Source Data file.

on genetic and molecular profiles to identify specific features that predict a favorable response to IL-1 $\beta$  inhibition.

In conclusion, further clinical trials of canakinumab in patients with CCUS or lower-risk MDS defined based on the IPSS-M classification will clarify whether the modulation of IL-1 $\beta$ -induced inflammation can improve these patients' peripheral blood cytopenias and reduce their risk of developing cardiovascular disorders, thus modifying the course of the disease.

## Methods

The research complies with all relevant ethical regulations: MD Anderson Cancer Center IRB-approved human sample protocol PA15-0926. This study was conducted at the University of Texas MD Anderson Cancer Center (Houston, TX, USA) and was approved by MD Anderson's Institutional Review Board. It was performed in accordance with the ethical principles of the World Medical Association Declaration of Helsinki. All patients provided informed written consent. This study is registered at ClinicalTrials.gov (NCT04239157, <https://clinicaltrials.gov/study/NCT04239157>). No deviations from the protocol occurred.

## Study design and participants

Between August 2020 and June 2023, patients with relapsed/refractory lower-risk MDS, defined as low or intermediate-1 risk by the International Prognostic Scoring System (IPSS)<sup>25</sup> or a score of  $\leq 3.5$  by the Revised IPSS (IPSS-R)<sup>26</sup>, with a hemoglobin level  $< 10$  g/dL and symptomatic anemia or transfusion dependency (defined as the need for transfusion eight weeks before treatment for hemoglobin levels less than 8 g/dL) were eligible for the study. Although the IPSS/IPSS-R was developed for untreated patients, its use in the risk stratification of patients with relapsed/refractory MDS was warranted, as no other prognostication tools are available.

Additional eligibility criteria included (1) age  $\geq 18$  years; (2) Eastern Cooperative Oncology Group (ECOG) performance status score  $\leq 2$ ; (3) completion of previous antineoplastic agents, including cytotoxic, biological, immunological, and investigational agents, at least 2 weeks before the start of the trial; and (4) adequate organ function (total bilirubin  $\leq 3.0 \times$  upper limit of normal [ULN], alanine aminotransferase and aspartate aminotransferase  $\leq 3.0 \times$  ULN, serum creatinine clearance  $> 30$  mL/min by the Cockcroft-Gault formula).

Sex-based analyses were not performed in the clinical trial. Males and females had comparable distributions in the clinical trial cohort. The sex of all patients is included in Supplementary Table 1. Gender is not relevant to this study. Due to the limited number of subjects enrolled in the clinical trial, disaggregated analysis by sex should be interpreted with caution.

Hydroxyurea was allowed for patients with rapidly proliferative disease at any time before or during the study if considered in the patient's best interest. However, none of the patients in the trial received hydroxyurea before or during canakinumab administration. Patients with previously untreated MDS, uncontrolled infection, or pregnancy/lactation were excluded.

## Procedure

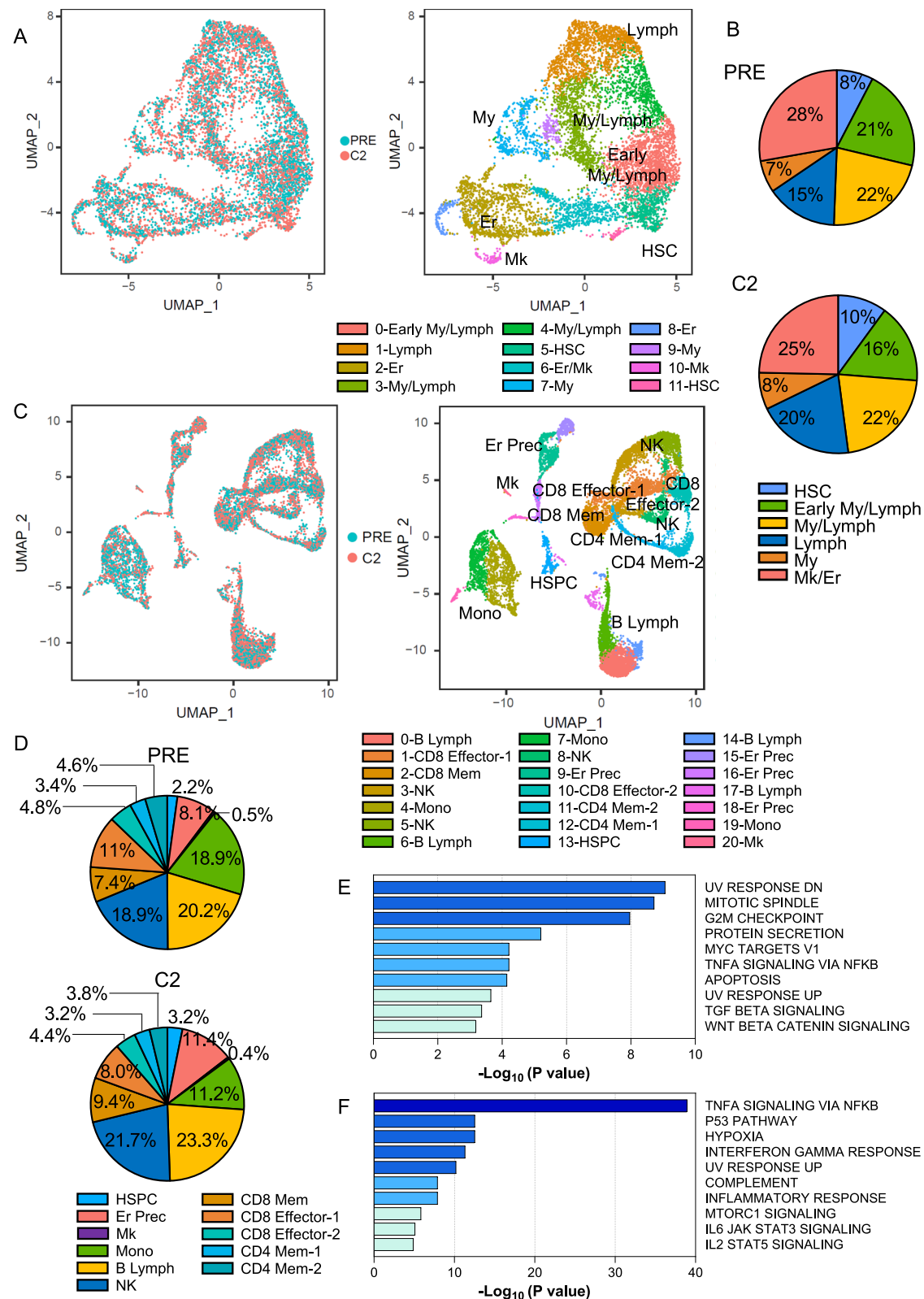
This was an open-label, single-arm, phase 2 clinical trial. Patients were enrolled from September 2020 through November 2022. Since canakinumab was not previously studied in MDS, we first performed a short exploratory dose-finding run-in phase using a standard 3 + 3 design with subcutaneous canakinumab given at 150 mg (first dose level) and then 300 mg (second dose level). After this first phase, all newly recruited patients received 300 mg of subcutaneous canakinumab. Canakinumab was supplied by Novartis (Basel, Switzerland) and administered subcutaneously on day 1 of a 4-week cycle. The study's primary endpoint was the clinical activity of canakinumab, which was determined by the rate of hematologic improvement (HI). Secondary objectives were the safety profile, including the rate of transfusion independence (TI), the duration of response (DoR), progression-free survival (PFS), leukemia-free survival (LFS), and overall survival (OS).

## Study assessments

Bone marrow (BM) aspirations and/or biopsies, flow cytometry, conventional cytogenetics, and mutation analyses using an 81-gene next-generation sequencing (NGS) panel<sup>33</sup> were performed before therapy. Additional BM aspirations and/or biopsies were performed at cycle 2, day 28 ( $\pm 3$  days), and then every three cycles after that or more frequently as clinically warranted. Unless no response was achieved after six or more cycles, canakinumab was continued until disease progression, unacceptable toxicity, the development of concurrent severe illness, patient refusal, or non-compliance. Safety was evaluated in all patients who received at least one canakinumab dose by adverse event (AE) assessment, clinical laboratory test results, physical examinations, and vital signs. AEs were graded according to the National Cancer Institute Common Terminology Criteria for Adverse Events (NCI-CTCAE) version 5.0.

## Single-cell RNA sequencing (scRNA-seq)

FACS-purified live lineage (Lin)<sup>+</sup>CD34<sup>+</sup> or BM mononuclear cells (MNCs) were processed and sequenced at MD Anderson's Advanced Technology Genomics Core, as previously described<sup>34</sup>. Sample concentration and cell suspension viability were evaluated using a Countess II FL Automated Cell Counter (ThermoFisher Scientific, Waltham, MA) and manual counting. Samples were normalized for input onto the



Chromium Single Cell A Chip Kit (10x Genomics, Pleasanton, CA), in which single cells were lysed and barcoded for reverse transcription. The pooled, single-stranded, barcoded cDNA was amplified and fragmented for library preparation. Pooled libraries were sequenced on a NovaSeq6000 SP 100-cycle flow cell (Illumina, San Diego, CA).

Sequencing analysis was performed using 10x Genomics' Cell Ranger software (v4.0.0 for samples UPN-07 and UPN-14 or v6.1.0 for all other samples). Fastq files were generated using the Cell Ranger

MkFastq pipeline. Raw reads were mapped to the human reference genome (refdata-cellranger-GRCh38-3.0.0) using the Cell Ranger Count pipeline. Intron reads were not counted. The digital expression matrix was analyzed with the R package Seurat (version 4.0.3-5.1.0)<sup>35</sup> to identify each cell type and signature gene. Cells with fewer than 500 unique molecular identifiers or greater than 50% mitochondrial expression were excluded from further analysis. The Seurat function NormalizedData was used to normalize the raw counts. Variable genes



**Fig. 4 | Canakinumab treatment fails to rescue anemia in patients with MDS with SF3B1 mutations. A** UMAP plot of scRNA-seq data from Lin<sup>+</sup>CD34<sup>+</sup> cells from the BM of patients UPN-07 and UPN-14 before canakinumab treatment (PRE;  $n = 3814$ ) and after 2 cycles (C2) of canakinumab treatment ( $n = 4043$ ). Each dot represents a single cell. Different colors represent the sample (left) and cluster (right) identities. Lymph, lymphoid; My, myeloid; Er, erythroid; HSC, hematopoietic stem cell; Mk, megakaryocytic. **B** Cluster distribution of Lin<sup>+</sup>CD34<sup>+</sup> cells isolated from the BM before canakinumab treatment (PRE) and during cycle 2 (C2) of canakinumab treatment, represented as the percentage of cells in each cluster shown in Fig. 4A. **C** UMAP plot of scRNA-seq data from BM MNCs isolated from patients UPN-07 and UPN-14 before canakinumab treatment (PRE;  $n = 6580$ ) and after 2 cycles (C2) of canakinumab treatment ( $n = 7356$ ). Different colors represent the sample (top) and cluster (bottom) identities. Er, erythroid; Prec, precursor; NK, natural killer; Mk, megakaryocytic; Mem, memory; HSPC, hematopoietic stem and

progenitor cell; Mono, monocytic; Lymph, lymphoid. **D** Cluster distribution of BM MNCs before canakinumab treatment (PRE) and at the end of cycle 2 (C2) of canakinumab treatment, represented as the percentage of cells in each cluster shown in Fig. 4C. HSPC, hematopoietic stem and progenitor cell; Mk, megakaryocytic; Mono, monocytic; Er, erythroid; Prec, precursor; NK, natural killer; Lymph, lymphoid. **E** Pathway enrichment analysis of genes significantly ( $P \leq 0.05$ ) downregulated in HSCs from patients UPN-07 and UPN-14 at the end of cycle 2 of canakinumab treatment compared with those in HSCs before canakinumab treatment. The top 10 Hallmark gene sets are shown. **F** Pathway enrichment analysis of genes significantly ( $P \leq 0.05$ ) downregulated in monocytes from patients UPN-07 and UPN-14 at the end of cycle 2 of canakinumab treatment compared with those in monocytes before canakinumab treatment. The top 10 Hallmark gene sets are shown. Source data are provided as a Source Data file.

were identified using the FindVariableFeatures function. The ScaleData function was used to scale and center expression values in the dataset, and the number of unique molecular identifiers was regressed against each gene. Uniform manifold approximation and projection (UMAP) was used to reduce the data dimensions, and the first two dimensions were used in the plots. The FindClusters function was used to cluster the cells. Marker genes for each cluster were identified using the FindAllMarkers function. Cell types were annotated based on the marker genes and their match to canonical markers<sup>36–39</sup>. Pathway analyses of differentially expressed genes were conducted using Metascape, based on the two-sided hypergeometric test. The Benjamini-Hochberg procedure is used for multiple comparison corrections<sup>40</sup>.

CellPhoneDB (v2.0.0)<sup>17</sup> was used to analyze ligand–receptor interactions. The connectome web was plotted using the igraph package in R.

### Quantification of cytokines, chemokines, and growth factors in BM plasma

EGF, eotaxin, G-CSF, GM-CSF, IFN- $\alpha$ 2, IFN- $\gamma$ , IL-1 $\alpha$ , IL-1 $\beta$ , IL-1RA, IL-2, IL-3, IL-4, IL-5, IL-6, IL-7, IL-8, IL-10, IL-12 (p40), IL-12 (p70), IL-13, IL-15, IL-17A, IL-17E/IL-25, IL-17F, IL-18, IL-22, IP-10, MCP-1, M-CSF, MIG, MIP-1 $\alpha$ , MIP-1 $\beta$ , PDGF-AA, PDGF-AB/BB, TNF- $\alpha$ , TNF- $\beta$ , VEGFA, and RANTES were simultaneously quantified from the plasma collected from the BM of patients enrolled in the clinical trials using the MILLIPLEX Human Cytokine/Chemokine/Growth Factor Panel A (HCYTA-60K-PX38, Millipore, Burlington, MA) according to the manufacturer's guidelines. Samples were assayed neat, and 50  $\mu$ L of a 1:1 mixture of the sample and assay buffer was added to each assay plate well. For the detection of RANTES, the samples were initially diluted with the assay buffer to 1:100. Briefly, 25  $\mu$ L of the 38-analyte bead mixture was added to each plate well, and the plate was incubated overnight at 4 °C. The following day, the plate was incubated at room temperature for 30 min with shaking at 500 rpm. After three washes, 25  $\mu$ L of detection antibody was added to each well, and the plate was incubated for 1 h at room temperature with shaking at 500 rpm. Then, 25  $\mu$ L of streptavidin–phycoerythrin solution was added to each well, and the plate was incubated for 30 min at room temperature with shaking at 500 rpm. After three wash steps, 150  $\mu$ L of xMAP Sheath Fluid Plus (4050021, Thermo Fisher, Waltham, MA) was added to each well. The acquisition was performed using the Luminex 200 system and xPO-NENT version 4.2 software. Analysis was performed using the Bio-Plex Manager version 6.1 software.

### Statistical analysis

Responses were assessed using the modified International Working Group 2006 criteria for MDS<sup>41</sup>. The overall response rate (ORR) included complete response (CR), marrow CR (mCR), hematological improvement (HI), and a combination of mCR and HI. The patients' demographic and clinical characteristics and safety data were summarized using descriptive statistics such as means and standard

deviations or medians and ranges. Toxicity type, severity, and attribution were summarized for each patient using frequency tables. For the efficacy analysis, we estimated the HI rate for canakinumab and the 95% confidential intervals (CIs) using the normal approximation method. Transfusion independence (TI) was defined as no transfusion requirements during an 8-week period or longer. The distribution of time-to-event endpoints (OS, PFS, LFS, and DoR) was estimated using the Kaplan–Meier method and compared using the log-rank test. The analysis was further strengthened using the Cox proportional hazards model. OS was defined as the time from the start of therapy to death or last follow-up, with patients alive at the time of the last follow-up censored without event. PFS was defined as the time from diagnosis to disease progression or death from MDS. LFS was defined as the time from the start of therapy to transformation to AML or death from any cause, whichever occurred first. DoR was defined as the time from the first response to the time of first objective documentation of disease progression or death from any cause, whichever occurred first. The median follow-up was determined using the reverse Kaplan–Meier method. Statistical analyses were performed using the R platform (version 4.2.2). Figures were generated using GraphPad Prism (version 10.0.0). Oncoplot visualization was performed using the software package ComplexHeatmap (version 2.14.0). Swimmers plot visualization was performed using the software packages swimplot (version 1.2.0) and ggplot2 (version 3.4.3). Fig. 3A and the graphical abstract were made using Biorender.com.

The sample size of this study after the run-in phase ensures that a posterior credible interval for the HI rate has a width of 0.27 at most under the assumption of a HI rate of 20%. The data cutoff date for this analysis was June 11, 2023. Data were reviewed and analyzed by the contract research organization and the authors; all authors had access to the primary clinical trial data.

### Experimental data analysis

Quantitative data were analyzed with GraphPad Prism 10 software (GraphPad, La Jolla, CA). Figure legends indicate the statistical tests used in each experiment. Statistically significant differences in the figures are indicated as \* $P < 0.05$ , \*\* $P < 0.01$ , \*\*\* $P < 0.001$ , and \*\*\*\* $P < 0.0001$ .

### Reporting summary

Further information on research design is available in the Nature Portfolio Reporting Summary linked to this article.

### Data availability

To respect participant confidentiality, the study clinical data are not publicly available. Requests for deidentified data should be directed to the corresponding author. The corresponding author will make the data available immediately upon request for scientific non-profit purposes and further elaboration. The granted access to the data will not have any time limitation. The study protocol is also available upon

request to the corresponding author. The datasets generated using scRNA-seq have been deposited under the accession code [GSE237148](https://www.ncbi.nlm.nih.gov/bioproject/1000000000). The remaining data are available within the Article, Supplementary Information, or Supplementary Data file. Source data are provided as a Source Data file. Source data are provided with this paper.

## Code availability

The R scripts and Seurat objects are available on the GitHub page: [https://github.com/mafeiyang/Canakinumab\\_LR-MDS](https://github.com/mafeiyang/Canakinumab_LR-MDS).

## References

- Balandrán, J. C., Lasry, A. & Aifantis, I. The role of inflammation in the initiation and progression of myeloid neoplasms. *Blood Cancer Discov.* **4**, 254–266 (2023).
- Ganan-Gomez, I. et al. Deregulation of innate immune and inflammatory signaling in myelodysplastic syndromes. *Leukemia* **29**, 1458–1469 (2015).
- Florez, M. A. et al. Clonal hematopoiesis: mutation-specific adaptation to environmental change. *Cell Stem Cell* **29**, 882–904 (2022).
- Hormaechea-Agulla, D. et al. Chronic infection drives Dnmt3a-loss-of-function clonal hematopoiesis via IFN $\gamma$  signaling. *Cell Stem Cell* **28**, 1428–1442.e1426 (2021).
- Mayer-Barber, K. D. & Yan, B. Clash of the Cytokine Titans: counter-regulation of interleukin-1 and type I interferon-mediated inflammatory responses. *Cell Mol. Immunol.* **14**, 22–35 (2017).
- Martín-Sánchez, F. et al. Inflammasome-dependent IL-1 $\beta$  release depends upon membrane permeabilisation. *Cell Death Differ.* **23**, 1219–1231 (2016).
- Weber, A., Wasiliew, P. & Kracht, M. Interleukin-1 (IL-1) pathway. *Sci. Signal.* **3**, cm1 (2010).
- Pietras, E. M. et al. Chronic interleukin-1 exposure drives haematopoietic stem cells towards precocious myeloid differentiation at the expense of self-renewal. *Nat. Cell Biol.* **18**, 607–618 (2016).
- Mitchell, C. A. et al. Stromal niche inflammation mediated by IL-1 signalling is a targetable driver of haematopoietic ageing. *Nat. Cell Biol.* **25**, 30–41 (2023).
- Svensson, E. C. et al. TET2-Driven clonal hematopoiesis and response to Canakinumab: an exploratory analysis of the CANTOS Randomized Clinical Trial. *JAMA Cardiol.* **7**, 521–528 (2022).
- McClatchy, J. et al. Clonal hematopoiesis related TET2 loss-of-function impedes IL1 $\beta$ -mediated epigenetic reprogramming in hematopoietic stem and progenitor cells. *Nat. Commun.* **14**, 8102 (2023).
- Burns, S. S. et al. IL-1r1 drives leukemogenesis induced by Tet2 loss. *Leukemia* **36**, 2531–2534 (2022).
- Woo, J. et al. Effects of IL-1 $\beta$  inhibition on anemia and clonal hematopoiesis in the randomized CANTOS trial. *Blood Adv.* **7**, 7471–7484 (2023).
- Mogilenko, D. A. et al. Comprehensive profiling of an aging immune system reveals clonal GZMK(+) CD8(+) T cells as conserved hallmark of inflammaging. *Immunity* **54**, 99–115.e112 (2021).
- Jonsson, A. H. et al. Granzyme K(+) CD8 T cells form a core population in inflamed human tissue. *Sci. Transl. Med.* **14**, eabo0686 (2022).
- Lasry, A. et al. An inflammatory state remodels the immune microenvironment and improves risk stratification in acute myeloid leukemia. *Nat. Cancer* **4**, 27–42 (2023).
- Efremova, M., Vento-Tormo, M., Teichmann, S. A. & Vento-Tormo, R. CellPhoneDB: inferring cell-cell communication from combined expression of multi-subunit ligand-receptor complexes. *Nat. Protoc.* **15**, 1484–1506 (2020).
- Hindy, G. et al. Increased soluble urokinase plasminogen activator levels modulate monocyte function to promote atherosclerosis. *J. Clin. Investig.* **132**. <https://doi.org/10.1172/jci158788> (2022).
- Rawat, K. et al. CCL5-producing migratory dendritic cells guide CCR5+ monocytes into the draining lymph nodes. *J. Exp. Med.* **220**. <https://doi.org/10.1084/jem.2022129> (2023).
- Ozga, A. J., Chow, M. T. & Luster, A. D. Chemokines and the immune response to cancer. *Immunity* **54**, 859–874 (2021).
- Luque-Martin, R. et al. IFN- $\gamma$  drives human monocyte differentiation into highly proinflammatory macrophages that resemble a phenotype relevant to Psoriasis. *J. Immunol.* **207**, 555–568 (2021).
- Wimmer, N. et al. Lymphotoxin  $\beta$  receptor activation on macrophages induces cross-tolerance to TLR4 and TLR9 ligands. *J. Immunol.* **188**, 3426–3433 (2012).
- Ridker, P. M. et al. Antiinflammatory therapy with Canakinumab for Atherosclerotic Disease. *N. Engl. J. Med.* **377**, 1119–1131 (2017).
- Ridker, P. M. et al. Effect of interleukin-1 $\beta$  inhibition with canakinumab on incident lung cancer in patients with atherosclerosis: exploratory results from a randomised, double-blind, placebo-controlled trial. *Lancet* **390**, 1833–1842 (2017).
- Greenberg, P. et al. International scoring system for evaluating prognosis in myelodysplastic syndromes. *Blood* **89**, 2079–2088 (1997).
- Greenberg, P. L. et al. Revised international prognostic scoring system for myelodysplastic syndromes. *Blood* **120**, 2454–2465 (2012).
- Bernard, E. et al. Molecular international prognostic scoring system for myelodysplastic syndromes. *NEJM Evid.* **1**, EV1-Doa2200008 (2022).
- Clough, C. A. et al. Coordinated missplicing of TMEM14C and ABCB7 causes ring sideroblast formation in SF3B1-mutant myelodysplastic syndrome. *Blood* **139**, 2038–2049 (2022).
- Winter, S. et al. Mutations in the splicing factor SF3B1 are linked to frequent emergence of HLA-DR(low/neg) monocytes in lower-risk myelodysplastic neoplasms. *Leukemia* **38**, 1427–1431 (2024).
- Schneider, M. et al. Activation of distinct inflammatory pathways in subgroups of LR-MDS. *Leukemia* **37**, 1709–1718 (2023).
- Basiorka, A. A. et al. The NLRP3 inflammasome functions as a driver of the myelodysplastic syndrome phenotype. *Blood* **128**, 2960–2975 (2016).
- Cluzeau, T. et al. Pro-inflammatory proteins S100A9 and tumor necrosis factor- $\alpha$  suppress erythropoietin elaboration in myelodysplastic syndromes. *Haematologica* **102**, 2015–2020 (2017).
- Kanagal-Shamanna, R. et al. Principles of analytical validation of next-generation sequencing based mutational analysis for hematologic neoplasms in a CLIA-certified laboratory. *Expert Rev. Mol. Diagn.* **16**, 461–472 (2016).
- Rodriguez-Sevilla, J. J. et al. Hematopoietic stem cells with granulomonocytic differentiation state overcome venetoclax sensitivity in patients with myelodysplastic syndromes. *Nat. Commun.* **15**, 2428 (2024).
- Stuart, T. et al. Comprehensive integration of single-cell data. *Cell* **177**, 1888–1902.e1821 (2019).
- Laurenti, E. et al. The transcriptional architecture of early human hematopoiesis identifies multilevel control of lymphoid commitment. *Nat. Immunol.* **14**, 756–763 (2013).
- Laurenti, E. et al. CDK6 levels regulate quiescence exit in human hematopoietic stem cells. *cell stem cell* **16**, 302–313 (2015).
- Velten, L. et al. Human haematopoietic stem cell lineage commitment is a continuous process. *Nat. Cell Biol.* **19**, 271–281 (2017).
- Belluschi, S. et al. Myelo-lymphoid lineage restriction occurs in the human haematopoietic stem cell compartment before lymphoid-primed multipotent progenitors. *Nat. Commun.* **9**, 4100 (2018).
- Zhou, Y. et al. Metascape provides a biologist-oriented resource for the analysis of systems-level datasets. *Nat. Commun.* **10**, 1523 (2019).
- Cheson, B. D. et al. Clinical application and proposal for modification of the International Working Group (IWG) response criteria in myelodysplasia. *Blood* **108**, 419–425 (2006).

## Acknowledgements

This study was funded by Novartis (Basel, Switzerland). This work was supported by philanthropic contributions to MD Anderson's AML and

MDS Moon Shot Program and the Edward P. Evans Foundation. J.J.R.-S. is a recipient of MD Anderson's Odyssey Fellowship. This work used MD Anderson's South Campus Flow Cytometry and Cell Sorting Core Laboratory, ORION Core, and Sequencing and Microarray Facility, all of which are supported in part by the National Institutes of Health/National Cancer Institute through MD Anderson's Cancer Center Support Grant (P30 CA16672). The authors thank Joseph Munch for assistance with manuscript editing. We thank the patients who participated in this trial, their families, and the clinical and research staff at MD Anderson Cancer Center. The sponsor had no role in the study design, data collection interpretation, or manuscript writing.

## Author contributions

J.J.R.-S., V.A., K.S.C., G.M.-B., H.Y., J.J., X.C., and K.B. collected and curated the clinical data. S.L. provided pathological interpretation of the clinical samples and correlative molecular data. G.G.-M. designed the clinical study. F.M. analyzed the scRNA-seq data. X.H. performed the biostatistical analyses. V.A. and S.C. designed and interpreted all biological studies. J.J.R.-S., and S.C. wrote the manuscript.

## Competing interests

G.G.-M. declares research funding from Astex Pharmaceuticals, Novartis, Abbvie, BMS, Genentech, Aprea Therapeutics, Curis, Gilead Sciences; consulting fees from Astex Pharmaceuticals, Acceleron Pharma, and BMS; and payments or honoraria from Astex Pharmaceuticals, Acceleron Pharma, Abbvie, Novartis, Gilead Sciences, Curis, Genentech, and BMS. All other authors declare no competing interests.

## Additional information

**Supplementary information** The online version contains supplementary material available at <https://doi.org/10.1038/s41467-024-54290-2>.

**Correspondence** and requests for materials should be addressed to Simona Colla.

**Peer review information** *Nature Communications* thanks Shahram Kordasti, Elena Torre, Hong Wang, and the other, anonymous, reviewer(s) for their contribution to the peer review of this work. A peer review file is available.

**Reprints and permissions information** is available at <http://www.nature.com/reprints>

**Publisher's note** Springer Nature remains neutral with regard to jurisdictional claims in published maps and institutional affiliations.

**Open Access** This article is licensed under a Creative Commons Attribution-NonCommercial-NoDerivatives 4.0 International License, which permits any non-commercial use, sharing, distribution and reproduction in any medium or format, as long as you give appropriate credit to the original author(s) and the source, provide a link to the Creative Commons licence, and indicate if you modified the licensed material. You do not have permission under this licence to share adapted material derived from this article or parts of it. The images or other third party material in this article are included in the article's Creative Commons licence, unless indicated otherwise in a credit line to the material. If material is not included in the article's Creative Commons licence and your intended use is not permitted by statutory regulation or exceeds the permitted use, you will need to obtain permission directly from the copyright holder. To view a copy of this licence, visit <http://creativecommons.org/licenses/by-nc-nd/4.0/>.

© The Author(s) 2024

Juan Jose Rodriguez-Sevilla<sup>1,6</sup>, Vera Adema<sup>1,6</sup>, Kelly S. Chien<sup>1,6</sup>, Sanam Loghavi<sup>2</sup>, Feiyang Ma<sup>3</sup>, Hui Yang<sup>1</sup>, Guillermo Montalban-Bravo<sup>1</sup>, Xuelin Huang<sup>4</sup>, Xavier Calvo<sup>5</sup>, Joby Joseph<sup>1</sup>, Kristy Bodden<sup>1</sup>, Guillermo Garcia-Manero<sup>1</sup> & Simona Colla<sup>1</sup>✉

<sup>1</sup>Department of Leukemia, The University of Texas MD Anderson Cancer Center, Houston, TX, USA. <sup>2</sup>Department of Hematopathology, The University of Texas MD Anderson Cancer Center, Houston, TX, USA. <sup>3</sup>Department of Molecular, Cell and Developmental Biology, University of California Los Angeles, Los Angeles, CA, USA. <sup>4</sup>Department of Biostatistics, The University of Texas MD Anderson Cancer Center, Houston, TX, USA. <sup>5</sup>Laboratori de Citologia Hematològica, Servei de Patologia, Grup de Recerca Translacional Neoplàsies Hematològiques (GRETNHE), Hospital del Mar Research Institute (IMIM), Barcelona, Spain. <sup>6</sup>These authors contributed equally: Juan Jose Rodriguez-Sevilla, Vera Adema, Kelly S. Chien. ✉ e-mail: [scolla@mdanderson.org](mailto:scolla@mdanderson.org)